

Controllable deposition distance of aligned pattern via dual-nozzle near-field electrospinning

Cite as: AIP Advances **7**, 035310 (2017); <https://doi.org/10.1063/1.4974936>

Submitted: 11 December 2016 . Accepted: 11 January 2017 . Published Online: 15 March 2017

Zhifeng Wang, Xindu Chen, Jun Zeng, Feng Liang, Peixuan Wu, and Han Wang 



View Online



Export Citation



CrossMark

ARTICLES YOU MAY BE INTERESTED IN

Continuous near-field electrospinning for large area deposition of orderly nanofiber patterns

Applied Physics Letters **93**, 123111 (2008); <https://doi.org/10.1063/1.2975834>

Fabrication and evaluation of controllable deposition distance for aligned pattern by multi-nozzle near-field electrospinning

AIP Advances **8**, 075111 (2018); <https://doi.org/10.1063/1.5032082>

Fabrication of various micro/nano structures by modified near-field electrospinning

AIP Advances **5**, 041301 (2015); <https://doi.org/10.1063/1.4901879>



AVS Quantum Science
A high impact interdisciplinary journal for **ALL** quantum science

ACCEPTING SUBMISSIONS

The advertisement features a red diagonal banner with the word "NEW". It includes the AIP Publishing logo and the AVS logo. To the right are several circular icons representing different fields of quantum science. The background is light blue.

Controllable deposition distance of aligned pattern via dual-nozzle near-field electrospinning

Zhifeng Wang, Xindu Chen, Jun Zeng, Feng Liang, Peixuan Wu,^a
and Han Wang^b

Guangdong Provincial Key Laboratory of Micro-Nano Manufacturing Technology and Equipment, School of Electromechanical Engineering, Guangdong University of Technology, Guangzhou 510006, China

(Received 11 December 2016; accepted 11 January 2017; published online 15 March 2017)

For large area micro/nano pattern printing, multi-nozzle electrohydrodynamic (EHD) printing setup is an efficient method to boost productivity in near-field electrospinning (NFES) process. And controlling EHD multi-jet accurate deposition under the interaction of nozzles and other parameters are crucial concerns during the process. The influence and sensitivity of various parameters such as the needle length, needle spacing, electrode-to-collector distance, voltage etc. on the direct-write patterning performance was investigated by orthogonal experiments with dual-nozzle NFES setup, and then the deposition distance estimated based on a novel model was compared with measurement results and proven. More controllable deposition distance and much denser of aligned naofiber can be achieved by rotating the dual-nozzle setup. This study can be greatly contributed to estimate the deposition distance and helpful to guide the multi-nozzle NFES process to accurate direct-write pattern in manufacturing process in future. © 2017 Author(s). All article content, except where otherwise noted, is licensed under a Creative Commons Attribution (CC BY) license (<http://creativecommons.org/licenses/by/4.0/>). [<http://dx.doi.org/10.1063/1.4974936>]

INTRODUCTION

With the development of micro-nano process technology, micro-nano devices have been ubiquitous in our daily life, especially those has organic nanostructure that shows superior mechanical and electrical properties, such as scaffolds for tissue engineering,^{1,2} epidermal electronics,^{3,4} flexible display,⁵ stretchable batteries⁶ and nanogenerator⁷ etc. Electrohydrodynamic (EHD) printing is an enormous potential technique to achieve high-precision organic pattern.⁸ And electrospinning (ES) as the main branches of EHD to fabricate large area nanofibrous membrane is most common application, including separation membranes in lithium-ion batteries,⁹ supercapacitors,¹⁰ chemical gas sensors¹¹ and catalytic supports¹² etc. However, owing to chaotic whipping, ES is unstable and lack of controllability to deposit accurately.¹³

Near-field electrospinning (NFES) is a revolution technology to write nanofibers in a direct, continuous, and controllable manner precisely by shortening working distance within 5.0 mm.¹⁴ Comparison with conventional methods to fabricate nanostructure, including electron beam lithography (EBL), focused ion beams (FIB), and dip-pen nanolithography (DPN) etc., high cost, special equipment and complex process are their limitation to broaden application.^{15–17} And NFES is a cost-effective, environmental friendly and wide material adaptability way to accurate deposit in biotechnology, electronics, microelectromechanical and energy. Fuh¹⁸ proposed highly flexible self-powered sensors can detect the motion and guest, which based on printed circuit board (PCB) technology by direct-write NFES. And in order to control cell alignment, NFES is used to direct-write parallel nanofibers patterns as fiber distance between 10 and 20 μm.¹⁹ In addition, NFES used to

^aAuthor to whom correspondence should be addressed. Electronic mail: peixuan@gdut.edu.cn;

^bAuthor to whom correspondence should be addressed. Electronic mail: wonghan0@163.com.

obtain the PVDF/PMLG nanofibers which have great piezoelectric properties to fabricate nanogenerator.^{20–22} Although NFES has incomparable advantages, the drawback of low production efficiency is obvious.^{23–25} Therefore, to increase productivity and practicality of NFES in simple and cost-effective way is an urgent and common requirement.

With multi-nozzle ES method,²⁶ the production rate by this approach is several times higher than single-needle ES setup. For example, Thirumal²⁷ proposed multi-nozzle far-field electrospinning (FFES) combined with an air-shield enclosed rotating drum collector to increase productivity effectively. And Needleless electrospinning process is another EHD system used multi-sharp-point as needles to improve productivity with porous tubes, wire coin, counter-electrode etc.²⁸ Therefore, to raise number of spinnerets is an potential and efficient way for mass production to fabricate nanofibers in NFES. However, because there are lots of parameters under the interaction of jet in multi-nozzle NFES, the uncertainty is larger than conventional ES process. Furthermore, few investigations on the interaction of the jet are carried on. With the dual-nozzle NFES process, the uncertainty is more suitable to investigate than the multi-nozzle NFES and also meets higher liquid throughput requirement than conventional ES process. In order to study the deposition characteristics of dual-nozzle NFES, the morphology and permutation of nanofiber is of great concern. Pan²⁹ proposed to rotate double-nozzle to fabricate parallel fibers with different distance, however, it is unable to deposit in determine distance. Moreover, Wang built a theoretical model to describe distance of double-nozzle NFES deposition about working distance, voltage, needle spacing and flow rate. But there is limitation on considering the vertical movement as a uniform motion with neglecting the effect of electric field in vertical direction caused by needles,³⁰ in addition, combing analogical method with experiment data to popularize above mentioned model to multi-needle NFES.³¹

In this paper, we present dual-nozzle NFES process for fabricating aligned nanofibers with different process parameters, including needle length, needle spacing, electrode-to-collector distance and working voltage etc. Together, under the interaction of the nozzles and other ES parameters, double charge jets are repulsed to spray as parabola and deposited on substrate as aligned nanofibers. With orthogonal experiments, the influence and sensitivity of ES parameters are investigated on deposition distance, and then deposition distance is estimated based on a theoretical model and compared with measurement results and proven. Moreover, to rotate the nozzles setup can be more controllable and dense to deposit aligned nanofibers in determined spacing. This work can be greatly contributed to estimate deposition distance and helpful to guide multi-nozzle NFES process to boost productivity in manufacturing aligned nanofibers in various fields.

MATERIALS AND METHODS

To study dual-nozzle NFES deposition characteristic further, the experiment setup system as shown in Fig. 1 was built with X-Y motion platform (SURUGA, Japan) and Z-axis linear platform (SURUGA, Japan) which can adjust collector speed ($V_c = 20\text{ mm/s}$ in constant), deposition location and electrode-to-collector distance respectively. And the syringe pump with constant flow rate ($V_f = 0.2\mu\text{m/min}$) was installed on shelf of the Z-axis linear platform. The dual-nozzle size is 28G, whose inner diameter is 0.18mm and outer diameter is 0.36mm with different needle length and spacing. The applied voltage was adjusted by programmable controlled high DC power source (DW-P503-1ACDF, Dongwen). Moreover, the motion of dual –nozzle NFES process is observed by CCD microscope (DCR-HC 28, SONY) and the collected nanofibers are observed with CNC video measuring system (VMS-3020H, whose resolution is $0.5\mu\text{m}$ and measuring accuracy ranges from $\pm 2\mu\text{m}$ to $\pm 3\mu\text{m}$) and Scanning Electron Microscopy (HITACHI TM3030). The experiments were performed at stable environmental condition whose ambient temperature as 20°C and relative humidity as 50%. The polymer solution of 5wt% ethylene oxide (PEO; $M_w = 2 \times 10^6\text{ g} \cdot \text{mol}^{-1}$; Aladdin Shanghai China) and the distilled water which is purchased from Watsons is used for experiments.

RESULTS AND DISCUSSION

Fig. 1 shows the experiment apparatus system for dual-nozzle NFES processing, and two aqueous and continuous PEO jets are ejected from Taylor Cone when needles are applied enough working

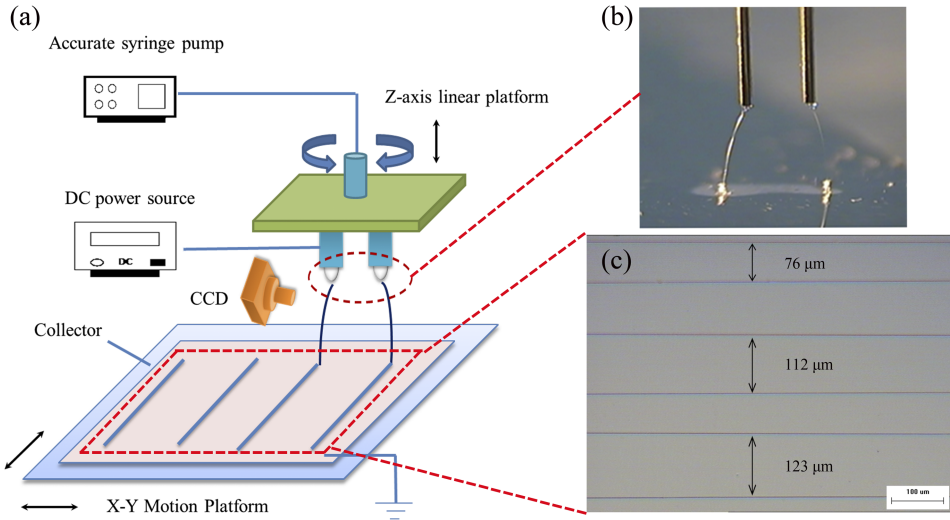


FIG. 1. (a) The schematic of dual-nozzle near-field electrospinning. (b) The flight process of charged jets. (c) Aligned nanofibers are direct-written by dual-nozzle NFES process with different rotatable angle.

voltage. In the flight process, the motion of charged jets is quasi-parabolic under-symmetrical as nozzles distribution due to Coulomb force caused by adjacent charged jets,²⁶ finally, they are deposited on substrate. With the tractive force by substrate, two deposited charged jets are straightened as aligned nanofibers in direct manner. Moreover, the dual-jets deposition process is multi-physics field coupling, including the electric field force caused by electrified needles and collector, including the needles, Coulomb force between charged jets, external resistance and gravitational force. Therefore, to study deposition distance with various process parameters in order to control deposit accurately is remarkable. The major process parameters are the needle length (L), needle spacing (D), electrode-to-collector distance (H) and voltage (U) etc.

To further investigate the influences and interaction between the various factors for deposition distance, a four-factor, three-level orthogonal experiment for dual-nozzle NFES is designed. Factors and levels are shown as Table I. With analysis of experiment data, the maximal value of error is 0.05, which indicates that these experimental results legitimately reflect the influence of various factors in dual-nozzle NFES process. Moreover, we could observe intuitively the sensitivity coefficient of influence parameters on deposition distance by bar chart as Fig. 2 shown, then, influence factors are listed in descending order as followed: needle spacing, Electrode-to-collector distance, needle length and voltage. And the influence of the combined effect of needle length and needle spacing is apparent, but the others are weaker.

More important, Fig. 3 demonstrates that deposition distance increases with an increase in needle length because the longer needles lead to larger surface and thus there are less charge in unit length with definite voltage, causing decrease in vertical component of electric field intensity as appendix shown, and resulting in longer dropping time. Therefore, deposition distance grows with comprehensive effect

TABLE I. The orthogonal array of electrospinning parameter.

Levels	Col.			
	A Needle length (inch)	B Needle spacing (mm)	C Voltage (kV)	D Electrode-to-collector distance(mm)
1	1/4	2.0	2.0	3.0
2	5/16	2.5	2.5	3.5
3	1/2	3.0	3.0	4.0

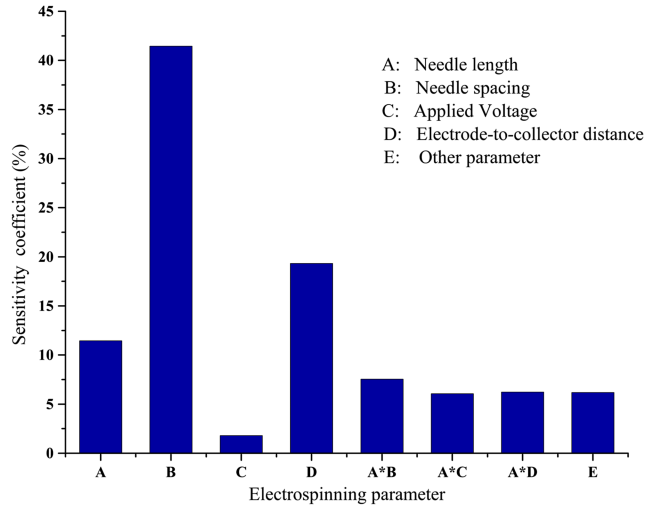


FIG. 2. The sensitivity coefficient of electrospinning parameter on deposition distance in dual-nozzle NFES process.

of needle length increases and definite horizontal force. Furthermore, the effect of applied voltage on deposition distance is unapparent as mentioned above and deposition distance approaches as a stable value. Owing to applied voltage increases with the increase in the electric field intensity between needles and substrate, and the direction of electrical field vector keep intact, thus, deposition distance enlarges with voltage increases, however, the deposition distance tends to stabilize in that cumulative charge of needles have reached its limit. Finally, experiments have shown positive correlation between electrode-to-collector distance and deposition distance as Fig. 4 shown. To enlarge electrode-to-collector distance that vertical electric field intensity diminishes, then shorten the flight time and resulted in smaller deposition distance when horizontal factor is invariable.

In dual-nozzle NFES, the charge jets broke away from the Taylor Cone and traveled as Fig. 5(a) shown. With the motion of collector, two aligned nanofibers are direct-written by EHD jet printing. The

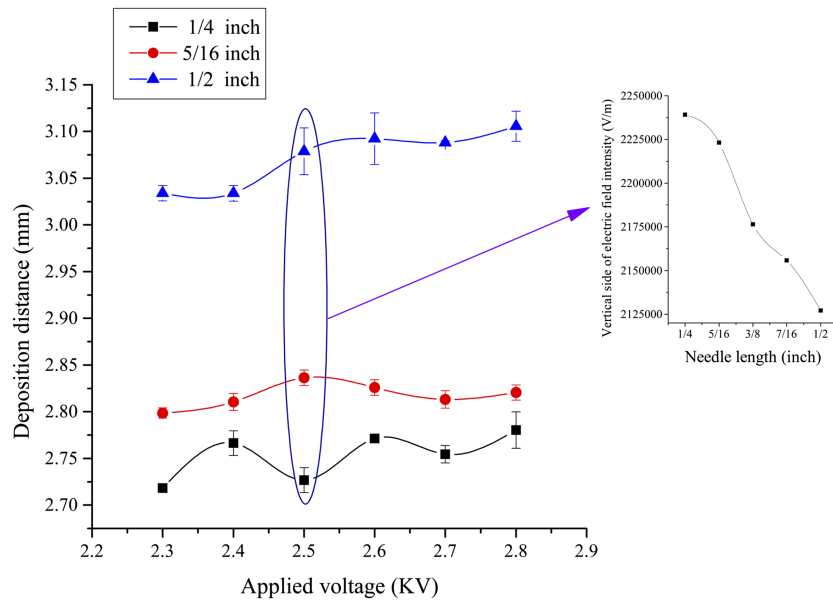


FIG. 3. Relationship between needle length, applied voltage and deposition distance. The nanofibers deposited in following condition: needle space 2.0 mm and electrode-to-collector distance is 4.0 mm. Moreover, appendix shows correction between needle length and vertical side of electric field intensity when applied voltage is 2.5KV.

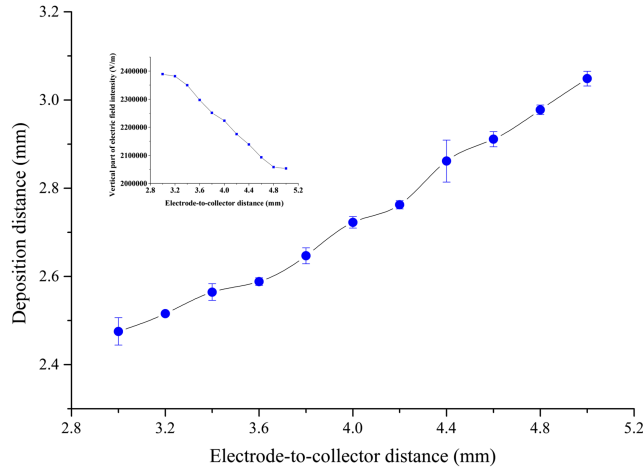


FIG. 4. The deposition distance and the vertical side of electric field intensity influenced by electrode-to-collector distance. The dual-nozzle NFES works in environment as: the needle length 5/16 inch and applied voltage 2.5 KV, and the vertical side of electric field intensity within electrode-to-collector distance as appendix shown.

charge jets can be assumed as bilateral symmetry. When the charge jets reach stable, the movement in near field can be considered as two-dimensional steady-element. Two-dimensional steady-state fluid model is used to analyze the behavior of the jet. Without considering the thermal effect, the charge jets were regarded as the one under the action of viscous stress, gravity, air resistance, surface tension, electric field force, Coulomb force and hydrostatic force as Fig. 5(b) showed.

Taking infinitesimal element from the charge jets into discussion, in the vertical direction X, the electric field force imposed on the microelement overwhelms the other forces, therefore, the vertical movement of the infinitesimal element in one of charge jets can be regarded as varying accelerated motion by electric field force. Moreover, the nozzle is considered as a uniform charged body whose cross-sectional radius is enough small. Because the microelement traveled in NFES process, the effect of the nozzle is far overweight the effect of neighboring nozzle which can be neglected. The electric field strength along the extension of needle $E(h)$ can be achieved, and h is the vertical distance from the tip of nozzle.

In vertical movement of the microelement, Wang³² accounted it as uniform motion to achieve the dropping time as following:

$$T = \frac{6\mu\rho Q\sigma z}{U^2}, \quad (1)$$

However, due to the effect of vertical component of electric field and the interaction with needles, it is unsuitable for regarding the vertical movement as the uniform motion. With the momentum

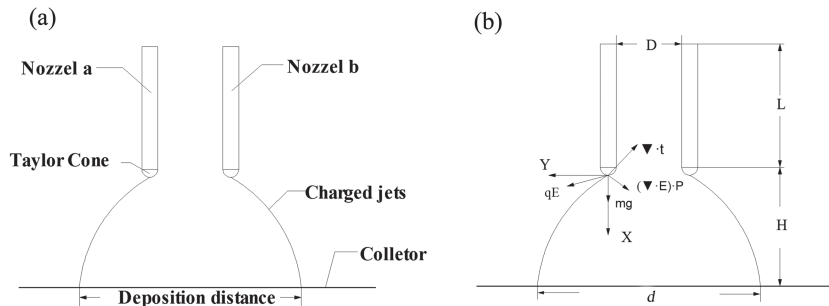


FIG. 5. Schematic representation of dual-nozzle NFES process.

theorem and $E(h)$, the vertical movement can be rewrote as following expression:

$$\int_0^H (L + h) h dh = \int_0^T \frac{qQ}{4\pi\epsilon m} \cdot t dt + C_1, \quad (2)$$

where ϵ is the permittivity of the air ($C^2/(Nm^2)$); q and Q is the quantity of electric charge of the microelement and single needle respectively (C), moreover, $Q = \lambda L$, which λ is the average charge per unit length (C/m); m is the quality of the microelement (kg); C_1 is constant value.

Therefore, the dropping time of the microelement from the Taylor Cone tip to the collector is simplified into Eq. (3):

$$T = \left(\frac{4\pi\epsilon m(3LH^2 + 2H^3) - C_1}{3qQ} \right)^{1/2} \quad (3)$$

In dual-nozzle NFES, the effect of electric field force is neglected because Coulomb force can be regarded as the prominent one acted on the lateral movement. The microelement from the jets can be regarded as a point charge. Following the principle of Coulomb's law and the momentum theorem, the deposition distance (d) can be expressed as:

$$\int_D^d r^2 dr = \int_0^T \frac{2kq^2}{m} \cdot t dt + C_2, \quad (4)$$

where k is Coulomb constant (Nm^2/C^2); and C_2 is constant value. The charge amount of the nozzle is almost proportional to the voltage, $Q \propto U$. According to the above analysis, the Eq. (5) can be rewritten as:

$$d = \left(\frac{K_r (3LH^2 + 2H^3 - C_1)}{U} + D^3 + 3C_2 \right)^{1/3}, \quad (5)$$

where K_r is the correction coefficient.

Although the influence and combined effect of needle spacing and needle length is apparent as above orthogonal experiment shown, it is difficult to adjust needle spacing and needle length in real-time during the experimental process and study on the relationships between the deposition distance and applied voltage or electrode-to-collector distance are more reasonable under current conditions.

To verify the proposed model, the Comparison with the experiment data and theoretical result under condition that $D = 2.0\text{ mm}$ and $L = 5/16\text{ inch}$. The relationship between the deposition distance and applied voltage whose $H = 4\text{mm}$ as Fig. 6(a) shown. The theoretical curve can be simplified as $d = (\frac{A}{U} + B)^{1/3}$, which $A = -3.3209 \times 10^4 V \cdot mm^3$ and $B = 36.1013 mm^3$. And the theoretical curve is accordance with the experimental one among the applied voltage. But the theoretical curve diverges

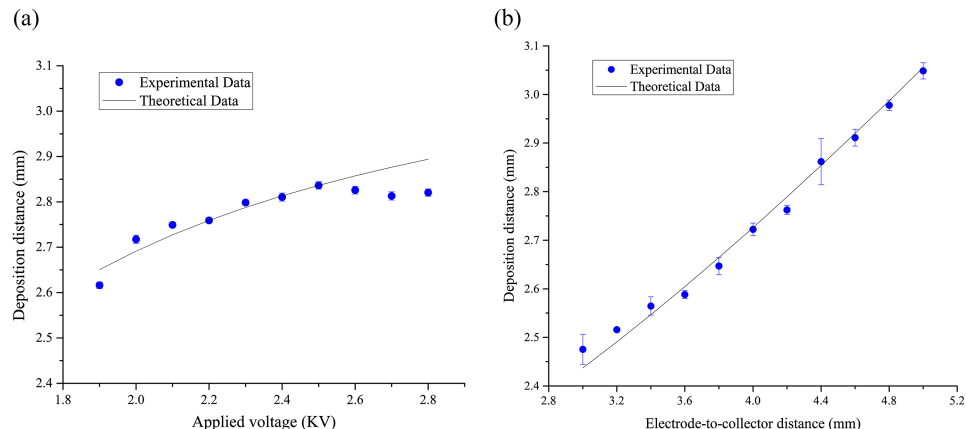


FIG. 6. The comparison on theoretical curve and experimental data. (a) The relationship between the deposition distance and applied voltage. (b) The relationship between the deposition distance and electrode-to-collector distance.

from the experiment curve when the applied voltage ranges from 2.5 KV to 2.8 KV because the size of Taylor cone is diminished with the increasing voltage. The smaller Taylor cone accumulates less charge and generates weaker electric repulsion to make deposition distance smaller than theoretical prediction.

Moreover, with applied voltage as $U = 2.5\text{ KV}$, the theoretical model describes the deposition distance with electrode-to-collector distance can be simplified as $d = (A \cdot (3LH^2 + 2H^3) + B)^{1/3}$, whose $A = 2.0816 \times 10^7$ and $B = 8.3316\text{ mm}^3$. From Fig. 6(b), the theoretical curve is almost in accordance with the experimental data ranging from 3.4 mm to 5.0 mm. However, the theoretical distance is smaller than the experimental date ranges from 3.0mm to 3.4mm because small electrode-to-collector distance generates strong electric repulsion and cause the deposition distance bigger.

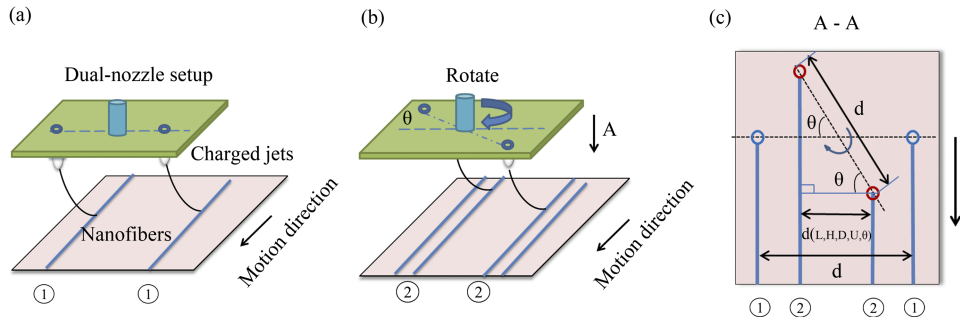


FIG. 7. The principle of method to improve nanofibers density. (a). $d(L, H, D, U, \theta) = d$, when $\theta = 0^\circ$; (b). the charged jets deposited on substrate in modified deposition distance when dual-nozzle setup rotated θ . (c). the relationship between deposition distance and modified deposition distance. And ①, ② show the deposition sequence during dual-nozzle NFES, respectively.

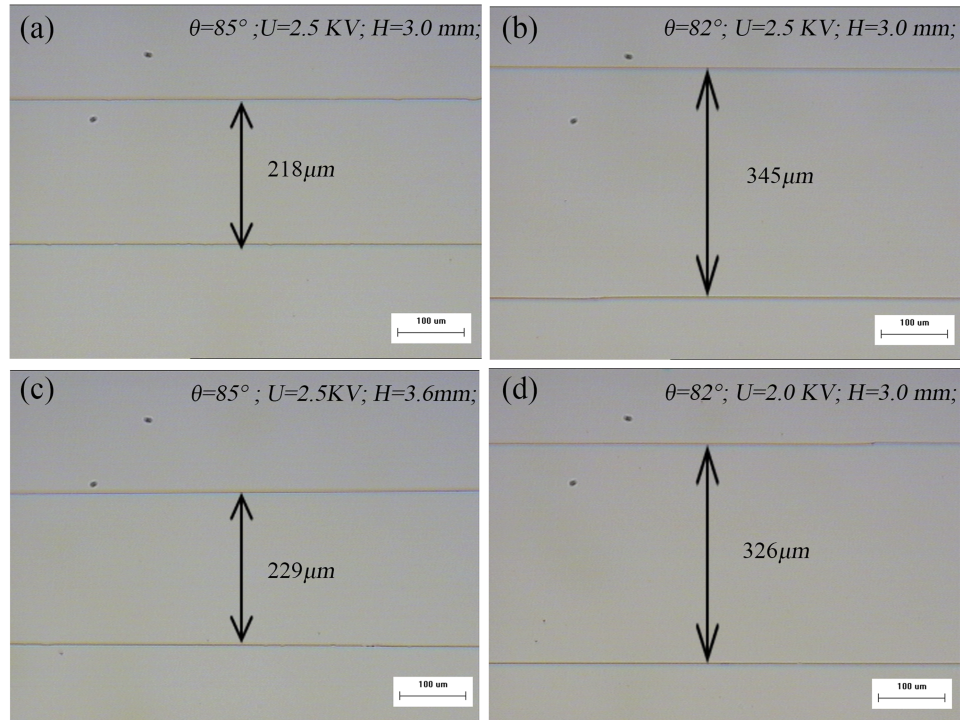


FIG. 8. Deposition distance of aligned nanofibers in different parameter, including rotational angle, voltage and electrode-to-collector distance. And $D=2\text{mm}$.

What is more important is to control the dual-nozzle NFES direct-write nanofiber density. We have rotated the dual-nozzle setup along the center of nozzles to control the nanofiber density abased above method. With the rotary table, nozzles are rotated θ , charged jets deposited aligned nanofibers on substrate and the rotational process as Fig. 7 (a) to Fig. 7 (b) shown. The rotational process leads to modified deposition distance $d(L, H, D, U, \theta)$ and the relationship between them as Fig. 7 shown and express as:

$$d(L, H, D, U, \theta) = \left(\frac{K_r(3LH^2 + 2H^3 - C_1)}{U} + D^3 + 3C_2 \right)^{1/3} \cdot \cos \theta \quad (6)$$

As shown in Fig. 8 (a)–(b), to rotate dual-nozzle setup leads to smaller deposition distance when rotation angle increase during θ ranges 0° from 90° . Moreover, it revisited to verify the principle of dual-nozzle NFES direct-writing on deposition distance with applied voltage, electrode-to-collector distance and rotational angle as Fig. 8 shown. Therefore, it is feasible to predict and control deposition distance of aligned nanofibers by direct-written in dual-nozzle NFES.

CONCLUSION

This paper investigated the deposition characteristic of dual-nozzle NFES by different process parameters, such as needle length, needle spacing, electrode-to-collector distance and voltage. And a theoretical model was proposed to describe deposition distance of the dual-nozzle NFES. The experiment and theoretical model verified that the deposition distance increases with the electrode-to-collector distance or voltage increasing. The experimental data almost coincides with theoretical prediction in certain range. The results can be contributed to predict the deposition distance and to rotate nozzles setup to achieve more controllable deposition distance and much denser nanofibers. This study can guide the dual-nozzle NFES in manufacturing process, and also illustrate the force distribution of the jet with multi-field coupling in future.

ACKNOWLEDGMENTS

This work was financially supported by National Natural Science Foundation of China (No. 51305084), Guangdong Innovative Research Team Program (No. 201001G0104781202), Guangdong Innovative Research Team Program (No. 2014ZT05G157), Project of Science and Technology of Guangdong Province, China (No. 2013B011301005), Guangdong Provincial Key Laboratory of Micro-nano Manufacturing Technology and Equipment(GDMNML2013-1), Key Project of Science and Technology of Guangdong Province, China (No. 2015B010124001), Guangdong Provincial Key Laboratory Construction Project of China (Grant No. 2011A060901026), Key Joint Project of National Natural Science Foundation of China (Grant No. U1134004), Project of Science and Technology of Guangdong Province (No. 2015B010102014).

- ¹ R. Balen, W. V. da Costa, J. de Lara Andrade, J. F. Piai, E. C. Muniz, and M. V. Companhoni, *Applied Surface Science* **385**, (2016).
- ² D. I. Braghirilli, D. Steffens, and P. Pranke, *Drug Discovery Today* **19**, 6 (2014).
- ³ S. H. Park, H. B. Lee, S. M. Yeon, J. Park, and N. K. Lee, *ACS Applied Materials & Interfaces* **8**, 37 (2016).
- ⁴ A. H. Najafabadi, A. Tamayol, N. Annabi, M. Ochoa, P. Mostafalu, and M. Akbari, *Advanced Materials* **26**, 33 (2014).
- ⁵ S. I. Park, Y. Xiong, R. H. Kim, P. Elvikis, M. Meitl, and D. H. Kim, *Science* **325**, 5943 (2009).
- ⁶ S. Xu, Y. Zhang, J. Cho, J. Lee, X. Huang, and L. Jia, *Nature Communications* **4**, 1543 (2003).
- ⁷ Q. Yang, D. Wang, M. Zhang, T. Gao, H. Xue, and Z. Wang, *Journal of Alloys and Compounds* **688** (2016).
- ⁸ J. U. Park, M. Hardy, S. J. Kang, K. Barton, K. Adair, and D. Kishore Mukhopadhyay, *Nature Materials* **6**, 10 (2007).
- ⁹ X. Zhang, L. Ji, O. Toprakci, Y. Liang, and M. Alcoutlabi, *Polymer Reviews* **51**, 3 (2011).
- ¹⁰ Y. E. Miao, W. Fan, D. Chen, and T. Liu, *ACS Applied Materials & Interfaces* **5**, 10 (2013).
- ¹¹ J. Shin, S. J. Choi, I. Lee, D. Y. Youn, C. O. Park, and J. H. Lee, *Advanced Functional Materials* **23**, 19 (2013).
- ¹² W. H. Ryu, T. H. Yoon, S. H. Song, S. Jeon, Y. J. Park, and I. D. Kim, *Nano Letters* **13**, 9 (2013).
- ¹³ N. J. Pinto, A. T. Johnson, Jr., A. G. MacDiarmid, C. H. Mueller, N. Theofylaktos, and D. C. Robinson, *Applied Physics Letters* **83**, 20 (2003).
- ¹⁴ D. Sun, C. Chang, S. Li, and L. Lin, *Nano Letters* **6**, 4 (2006).
- ¹⁵ A. A. Tseng, K. Chen, C. D. Chen, and K. J. Ma, *IEEE Transactions on Electronics Packaging Manufacturing* **26**, 2 (2003).
- ¹⁶ A. A. Tseng, *Small* **1**, 10 (2005).
- ¹⁷ K. Salaita, Y. Wang, and C. A. Mirkin, *Nature Nanotechnology* **2**, 3 (2007).
- ¹⁸ Y. K. Fuh and H. C. Ho, *Nanotechnology* **27**(9), 095401 (2016).

- ¹⁹ Y. K. Fuh, Y. C. Wu, Z. Y. He, Z. M. Huang, and W. W. Hu, *Materials Science and Engineering: C* **62** (2016).
- ²⁰ Y. K. Fuh, J. C. Ye, P. C. Chen, H. C. Ho, and Z. M. Huang, *ACS Applied Materials & Interfaces* **7**, 31 (2015).
- ²¹ C. T. Pan, C. K. Yen, H. C. Wu, L. Lin, Y. S. Lu, J. C. Huang, and S. W. Kuo, *Journal of Materials Chemistry A* **3**, 13 (2015).
- ²² N. Bu, Y. Huang, Y. Ding, and Z. Yin, *Sensors and Materials* **28**, 7 (2016).
- ²³ L. M. Bellan and H. G. Craighead, *Journal of Manufacturing Science and Engineering* **131**, 3 (2009).
- ²⁴ C. Hellmann, J. Belardi, R. Dersch, A. Greiner, J. H. Wendorff, and S. Bahnmueller, *Polymer* **50**, 5 (2009).
- ²⁵ T. D. Brown, P. D. Dalton, and D. W. Hutmacher, *Advanced Materials* **23**(47), 5651 (2011).
- ²⁶ A. Varesano, R. A. Carletto, and G. Mazzuchetti, *Journal of Materials Processing Technology* **209**, 11 (2009).
- ²⁷ T. Krishnamoorthy, M. Z. Tang, A. Verma, A. S. Nair, D. Pliszka, S. G. Mhaisalkar, and S. Ramakrishna, *Journal of Materials Chemistry* **22**(5), 2166 (2012).
- ²⁸ H. Niu, X. Wang, and T. Lin, *Technology* (2011).
- ²⁹ Y. Pan, Y. Huang, N. Bu, and Z. Yin, *Journal of Physics D: Applied Physics* **46**(25), 255301 (2013).
- ³⁰ H. Wang, M. Li, S. N. Huang, J. W. Zheng, X. Chen, and Z. M. Zhu, *Applied Physics A* **118**(2), 621 (2014).
- ³¹ H. Wang, S. Huang, F. Liang, P. Wu, M. Li, S. Lin, and X. Chen, *Journal of Nanomaterials* **16**, 1 (2015).
- ³² W. Han, L. Minhao, C. Xin, Z. Junwei, C. Xindu, and Z. Ziming, *AIP Advances* **5**, 4 (2015).